Check for updates

Chemistry & Biodiversity

CHEMISTRY & BIODIVERSITY

RESEARCH ARTICLE

Phytochemical and Computational Discovery of Potent Xanthine Oxidase Inhibitors From *Ziziphus lotus* L. Leaves and Seeds

Fatna Bellahcene[1,2] | Khedidja Benarous[1,2] | Ebru Erol[3] | Talia Serseg[1,2] | Gülaçtı Topçu[4,5] | Abderahmane Linani[2,6] | Hicham Bouakkaz[1] | Alaeddine Kaouka[2] | Mohamed Yousfi[1]

[1]Fundamental Sciences Laboratory, Faculty of Sciences, Amar Telidji University, Laghouat, Algeria | [2]Laboratory of Applied Sciences and Didactic, Higher Normal School of Laghouat, Laghouat, Algeria | [3]Department of Analytical Chemistry, Faculty of Pharmacy, Bezmialem Vakif University, İstanbul, Türkiye | [4]Department of Pharmacognosy, Faculty of Pharmacy, Bezmiâlem Vakıf University, İstanbul, Türkiye | [5]Drug Application and Research Center (DARC), Bezmiâlem Vakif University, İstanbul, Türkiye | [6]Department of Dental Medicine, University of Ghardaia, Ghardaia, Algeria

Correspondence: Fatna Bellahcene (f.belahcen@lagh-univ.dz) | Khedidja Benarous (k.benarous@lagh-univ.dz)

Received: 1 July 2025 | **Revised:** 13 October 2025 | **Accepted:** 17 October 2025

Keywords: ADMET | inhibitory | liquid chromatography–high-resolution electrospray ionisation mass spectrometry (LC–HRESIMS) | xanthine oxidase | *Ziziphus lotus*

ABSTRACT

Ziziphus lotus (L.), traditionally recognised for its anti-inflammatory and antioxidant properties, has received limited scientific exploration regarding its potential as an antigout agent. This study provides the first investigation of the inhibitory capacity of *Z. lotus* seed and leaf extracts against bovine xanthine oxidase (BXO), a key enzyme in uric acid biosynthesis and the pathogenesis of gout. To characterise its bioactive constituents, the potent extract was subjected to liquid chromatography–high-resolution electrospray ionisation mass spectrometry (LC–HRESIMS)-based phytochemical profiling. In vitro evaluation confirmed potent inhibitory effects, with the seed extract ($IC_{50} = 40.63 \pm 0.41$ µg/mL) showing superior activity over the leaf extract ($IC_{50} = 61.06 \pm 1.15$ µg/mL). LC–HRESIMS profiling of the seed extract identified fourteen metabolites, dominated by syringic acid (16 240.00 µg/g extract), sinapinic acid (3688.80 µg/g extract), and rutin (1918.00 µg/g extract) as the major constituents. A computational study focused on phytochemicals not previously assessed against XO; molecular docking demonstrated strong binding interactions to the target protein, suggesting promising inhibitory potential. ADMET and drug-likeness assessments highlighted (+)-*trans* taxifolin as the most promising candidate for drug development. Overall, these findings establish *Z. lotus* seeds as a valuable source of natural xanthine oxidase inhibitors and underscore their potential as novel phytotherapeutic agents for treating gout and hyperuricemia.

1 | Introduction

Herbal medicine has historically relied on plants as one of the most accessible and affordable sources of therapeutic agents in primary healthcare [1]. For millennia, they have provided a vast repertoire of remedies to prevent, manage, and alleviate diverse health conditions, establishing their enduring value in both traditional and modern medical practices [2]. *Ziziphus lotus* L., commonly known as wild jujube, belongs to the Rhamnaceae family, which comprises approximately 135–170 species within the *Ziziphus* genus. The plant is widely distributed across China, Iran, Africa, South Korea, and Europe, like Cyprus, Spain, and Sicily [3]. Although *Z. lotus* is common throughout Morocco, Tunisia, and other arid to semi-arid regions of the Mediterranean

© 2025 Wiley-VHCA AG, Zurich, Switzerland

basin, it is especially common in North Africa, especially in Mediterranean nations like Algeria, where it is known locally as 'Sedra' and yields the edible fruit 'Nbeg' [4]. Its fruits and leaves have been extensively employed in traditional medicinal practices to address a variety of health issues, including diabetes, diarrhea, bronchitis, abscesses, liver problems, and urinary and skin infections [5]. Based on the literature, the *Ziziphus* genus is phytochemically rich in saponins, tannins, flavonoids, alkaloids, and a wider variety of phenolic compounds responsible for its biological effects [6]. Recent scientific studies have further confirmed these ethnomedicinal uses by revealing the plant's rich phytochemical composition, which underpins its broad spectrum of pharmacological effects, including potent antioxidant capacity [7], anti-inflammatory activity [8], antihyperlipidemic effect [9], antimicrobial activity [10], antidiabetic [11], immune modulation [12], and neuroprotection [13].

Gout, a systemic disease, arises from the deposition of monosodium urate (MSU) crystals in various tissues, a consequence of elevated serum uric acid levels [14]. Uric acid is the terminal product of purine metabolism, synthesised via the catalytic action of xanthine oxidase (XO), which catalyses the oxidation of hypoxanthine to xanthine and subsequently to uric acid. This enzymatic process concurrently generates reactive oxygen species (ROS), such as hydrogen peroxide (H_2O_2) and superoxide anion ($O_2^{\bullet-}$), further exacerbating oxidative stress and inflammation [15]. A key therapeutic strategy for gout involves the use of xanthine oxidase inhibitors (XOIs) such as allopurinol and febuxostat [16], which reduces uric acid production [17]. However, their clinical use is often constrained by adverse effects, including neutropenia and susceptibility to infection [18], which has encouraged the search for safer natural XOIs from medicinal plants [19].

To the best of our knowledge, this is the first study to systematically investigate the antigout potential of *Z. lotus* ethyl acetate seed and leaf extracts through in vitro assessment of their xanthine oxidase inhibitory properties. The most active extract was subsequently subjected to comprehensive phytochemical profiling using liquid chromatography–high-resolution electrospray ionisation mass spectrometry (LC–HRESIMS). Moreover, in silico analyses were performed through PASS evaluation, ADMET and drug likeness prediction, pharmacophore modelling, molecular docking, and molecular dynamics (MD) simulation to elucidate the pharmacokinetic properties and binding interactions of the identified phytochemicals, thereby highlighting novel candidates with potential xanthine oxidase inhibitory activity.

2 | Materials and Methods

2.1 | Organics and Chemicals

Bovine milk was obtained from a local firm in Laghouat, Algeria. Uricase and peroxidase enzymes were purchased from BioLab. The substrate (xanthine), K_2HPO_4, KH_2PO_4, DMSO, HEPES, Tris, EDTA, and all other reagents were purchased from Sigma-Aldrich. All reagents used in the experiments were of analytical grade.

2.2 | Plant Collection

Dried leaves of *Z. lotus* were acquired in March 2023, while the dried seeds were obtained in September 2023 from a certified local herbalist located in Laghouat, Algeria. The plant material was authenticated by Pr. Khedidja Benarous, and voucher specimens for the leaves (ID: Zll/03.2023) and seeds (ID: Zls/09.2023) were deposited in the Herbarium of the University of Amar Telidji, Fundamental Sciences Laboratory, for future reference. All samples underwent quality inspection, were cleaned to eliminate impurities, air-dried at ambient temperature, and ground into a fine powder before extraction and subsequent analyses.

2.3 | XO Extraction

The extraction process involves a series of successive phases. For bovine xanthine oxidase (BXO), we followed the methodology described in the reference [20], with minor changes. A volume of 1.7 L of fresh and unpasteurised bovine milk obtained from a single cow was used in our experiments. Initially, the milk was centrifuged for 35 min at 4500 rpm at +4°C [21]. Subsequently, a floating white cream was assembled and briefly subjected to a temperature of 37°C, after which it was dissolved in a double volume of phosphate potassium (K_2HPO_4, 0.2 M) solution containing 1 mM of EDTA [22]. Following a 2-h period of agitation, the mixture was centrifuged at 6000 rpm for 20 min at 4°C [23]. The process was concluded with the acquisition of enzyme fractions, which were subjected to filtration and then collected [21, 24]. To ensure long-term stability and retain enzymatic activity, the XO extract was lyophilised. The extract was initially frozen at −50°C for 1 h to facilitate solidification. Subsequently, the frozen water content was removed through sublimation under controlled conditions (20–30°C, $p = 0.05$ mbar) for a total duration of 8 h. This process enabled the direct transition of ice from the solid to the vapour phase, ensuring efficient dehydration while minimising thermal and structural degradation of the enzyme [25].

2.4 | Plant Extraction

The dried seeds and leaves of *Z. lotus* were macerated in a ternary solvent system of ethanol–methanol–water (EtOH–MeOH–H_2O; 5:4:1, v/v/v) at room temperature for 48 h to ensure exhaustive extraction of both polar and nonpolar phytoconstituents. This solvent system was selected to maximise the recovery of diverse bioactive constituents by enabling efficient solubilisation of compounds with varying polarities. Following maceration, the mixture solution was filtered, and the alcoholic phase was evaporated using a rotary evaporator under reduced pressure at 40°C. The remaining aqueous fraction was subsequently subjected to liquid–liquid extraction with hexane and ethyl acetate, thereby fractionating metabolites according to their polarity. The obtained extracts were dehydrated using Na_2SO_4, filtered, and concentrated under reduced pressure at a temperature of 40°C. The resulting crude extracts were stored at 4°C until further analysis.

16121880, 2026, 1, Downloaded from https://onlinelibrary.wiley.com/doi/10.1002/cbdv.202502169 by Beam-I Abou Vakif University, Wiley Online Library on [07/01/2026]. See the Terms and Conditions (https://onlinelibrary.wiley.com/terms-and-conditions) on Wiley Online Library for rules of use; OA articles are governed by the applicable Creative Commons License

2.5 | Phytochemical Composition Using LC–HRESIMS

LC–HRESIMS analysis was performed using a Thermo Orbitrap Q-Exactive mass spectrometer to identify and quantify the phenolic compounds present in the ethyl acetate fraction of *Z. lotus seeds*. Compound separation was achieved with a Troyasil-C18 column (150 mm × 3 mm, 5 µm particle size) using chromatographic techniques. The LC–HRESIMS conditions followed those outlined in a previous study [26, 27]. Electrospray ionisation (ESI) was selected as the ionisation method due to its excellent performance with small polar molecules. In high-resolution mode, the mass spectrometer scanned ions within the m/z range of 100–900. Identification of the compounds was based on retention times and HR–MS data, compared with reference standards. To address potential issues with repeatability due to external factors like ionisation consistency, dihydrocapsaicin was used as an internal standard during LC–HRESIMS measurements [28, 29].

2.6 | XO Inhibition

The inhibition assay was conducted following our previously reported protocol [30], with modifications made to optimise assay conditions. BXO activity was determined spectrophotometrically by measuring uric acid formation from a 0.06 mg/mL xanthine substrate at 505 nm using a Thermo Fisher Scientific microplate reader. The enzymatic environment was maintained using Tris (50 mmol/L) and HEPES (100 mmol/L) to promote optimal pH for enzyme activities. The reaction mixture was prepared by pre-incubating BXO solution at a concentration of 20 mg/mL with varying concentrations of *Z. lotus* seed or leaf ethyl acetate extracts at 37°C for 15 min. Then, xanthine was added to start the reaction, and it was allowed to proceed for 30 min. The detection of uric acid production was later accomplished through a double enzyme detection (DED) system, in which the oxidation product was integrated to yield quinonimine, yielding a distinctive pink colour. Control measurement was performed under identical conditions in the absence of inhibitor. The inhibitory activity of BXO was expressed as a percentage, calculated as follows, where AC represents the absorbance in the absence of the inhibitor and AE represents the absorbance in the presence of the inhibitor [21].

$$I\,(\%) = \left(\frac{\mathrm{AC} - \mathrm{AE}}{\mathrm{AC}}\right) \times 100$$

The IC_{50} value, defined as the concentration of inhibitor required to inhibit 50% of XO activity [31]. It was expressed in µg/mL and calculated from the inhibition ratio versus *Z. lotus* concentration curves by regression analysis [24]. The extracts' inhibitory potency was subsequently evaluated against febuxostat, a clinically approved XO inhibitor, which served as the reference standard.

2.7 | PASS Study

In the framework of this study, the PASS approach has been applied to predict the inhibitory activity of chemical compounds using SMILES data generated from the PubChem database due to its capability to effectively prioritise compounds for further in vitro experimental validation [32]. PASS (Prediction of Activity Spectra for Substances) is an advanced computational tool developed in 1995 to predict, with remarkable accuracy, the biological activities [33], underlying physiological mechanisms, and a wide range of potential toxicological effects, such as mutagenicity, carcinogenicity, and embryotoxicity, of diverse chemical compounds [34]. This software generates qualitative predictions by analysing the intrinsic properties of a compound, solely based on its molecular structure [35]. The activity profile of a compound is expressed through probable activity (Pa) and probable inactivity (Pi) values, derived from structure-activity relationship (SAR) analysis of over 205 000 compounds representing more than 3750 distinct biological activities [36]. The molecular structure of compounds is delineated using Multilevel Neighbours of Atoms (MNA) descriptors, which represent atom-centred fragments within the molecule without accounting for its stereochemical details [37]. These descriptors function as a linear notation, capturing the connectivity of atoms and incorporating hydrogen atoms based on their valency and partial charges while excluding the specification of bond types. The generation of an MNA descriptor is constrained by specific conditions: the molecule must contain a minimum of three carbon atoms, remain in a neutral state, and possess a molecular weight (MW) below 1250 Da [38]. It has established itself as an indispensable tool in forecasting novel pharmacological effects, such as antiulcer, antimetastatic, and anti-inflammatory activities, as well as providing insights into mechanisms of action, toxicity profiles, and the modulation of gene expression [39]. In this study, we focused on selecting two biological activities from the PASS database as the primary criteria for identifying potential antigout drug candidates. These included the predicted high probability of inhibiting XO enzyme and their ability to effectively treat gout.

2.8 | ADMET and Drug-Likeness (DL) Evaluation

Computational methodologies are transforming drug discovery, offering unprecedented efficiency in identifying, optimising, and evaluating new therapeutic candidates within pharmaceutical and biomedical research [40]. However, the high incidence of clinical trial failures remains a major challenge [41]. To address these limitations, the in silico prediction has become an essential strategy for early-stage drug evaluation [42]. Reliable pharmacokinetic profiling is vital not only for optimising drug dosages but also for recognising potential drug interactions and assessing toxicity, thereby reducing the risk of late-stage development failures [43]. In this study, the pharmacological potential of phytoconstituents derived from *Z. lotus* seed ethyl acetate extract was examined through ADMET screening combined with POM (Petra, Osiris, and Molinspiration) analysis.

2.8.1 | ADMET Screening

Pre-ADMET v2.0 (https://preadmet.qsarhub.com/) and the ADMETLab (https://admetmesh.scbdd.com/) were used to evaluate the pharmacokinetic and toxicological behaviour of the selected compounds. These platforms analyse molecular structures based on their SMILES notations, enabling the high-throughput prediction of important key pharmacokinetic

16121880, 2026, 1, Downloaded from https://onlinelibrary.wiley.com/doi/10.1002/cbdv.202502169 by Bezm-I Alem Vakif University, Wiley Online Library on [07/01/2026]. See the Terms and Conditions (https://onlinelibrary.wiley.com/terms-and-conditions) on Wiley Online Library for rules of use; OA articles are governed by the applicable Creative Commons License

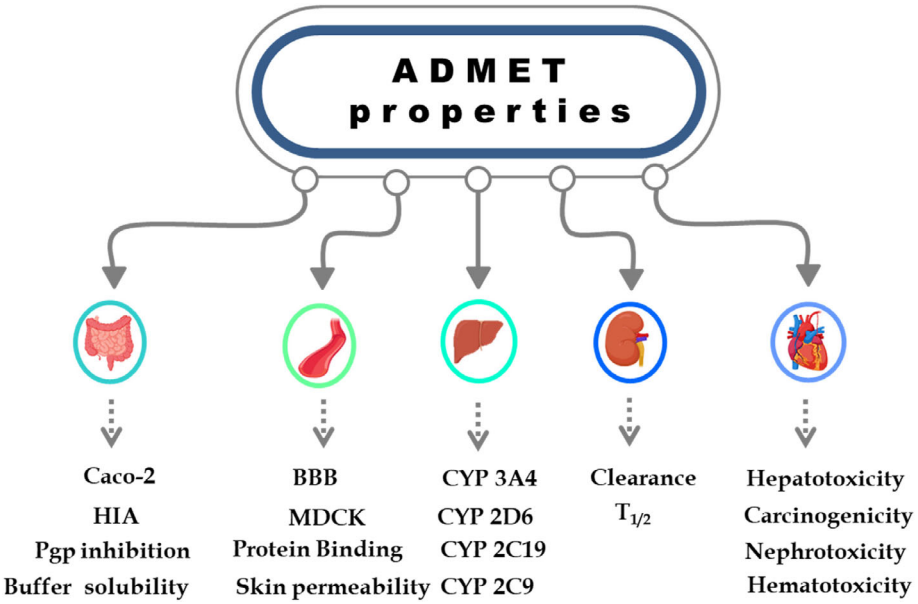

FIGURE 1 | Strategic selection of pharmacokinetic parameters for comprehensive ADMET profiling.

indices (absorption, distribution, metabolism, excretion and toxicity). These tools provided a rapid and cost-effective means of screening compounds, offering valuable insights into their pharmacological profiles, and facilitating the prioritisation of candidates for further experimental testing. The full set of pharmacokinetic parameters evaluated in this investigation is summarised in Figure 1.

2.8.2 | POM Analysis

POM analysis has been validated against approximately 7000 marketed drugs and is widely acknowledged for its capacity to produce two-dimensional models that pinpoint pharmacophore sites affecting biological activity in relation to structure [44]. This approach offers a robust framework for enhancing and defining the pharmacophoric characteristics of organic compounds based on physicochemical descriptors. Additionally, it facilitates the prediction of biological activities and the investigation of the connections between steric and electrostatic properties and biological activity [45]. Osiris Property Explorer, developed by Thomas Sander, predicts key physicochemical parameters, such as MW, cLog *P*, solubility in water (log *S*), and topological polar surface area (TPSA), while concurrently assessing toxicity risks, including mutagenicity, tumorigenicity, irritancy, and reproductive effects. These predictions are further integrated into calculations of DL and overall drug score (DS). Molinspiration Cheminformatics extends this analysis by supplying bioactivity scores across a range of therapeutic targets; it also offers cheminformatics tools for SMILES/SDfile conversion, tautomer generation, molecular normalisation, fragmentation, and descriptor computation necessary for QSAR modelling and structure-based drug design [46].

2.9 | Pharmacophore Modelling

Pharmacophore modelling involves the systematic identification of pivotal structural and spatial features within a molecule that influence its biological activity. It specifies the three-dimensional arrangement of essential chemical functionalities, such as hydrogen bond donors and acceptors, aromatic moieties, and hydrophobic regions that are responsible for creating optimal molecular interactions with the target biomacromolecule [47, 48]. In the present study, pharmacophore modelling was applied to forecast the distinctive characteristics of the ligands using ZINCPharmer (https://zincpharmer.csb.pitt.edu/), thereby shedding light on the chemical determinants that influence their inhibitory effectiveness against XO.

2.10 | Molecular Docking

Medicinal plants are distinguished by their vast repertoire of bioactive compounds, a characteristic that drives their wide-ranging and multifaceted therapeutic applications. In the present work, we performed an in-depth molecular docking analysis on two phytochemicals, (+)-*trans* taxifolin and luteolin-7-*O*-rutinoside newly identified in the *Z. lotus* seeds extract and not previously explored for their inhibitory potential against BXO in silico. In order to provide mechanistic insights into their potential therapeutic relevance, our research was intended to clarify their binding affinities and interaction patterns with the enzyme [49]. In structural molecular biology, molecular docking is one of the most important methods for predicting the preferred binding orientations of small molecules within macromolecular targets [50]. Beyond the prediction of ligand-protein interactions, this computational method generates valid structural hypotheses that can explain, at the atomic level, how natural substances affect or inhibit enzyme function in addition to discovering advantageous ligand-protein interactions [51]. It also makes it easier to find interesting drug candidates by offering important information about their binding affinities and modes of action by mimicking the docking process [52]. To accomplish these goals, comprehensive molecular docking analysis was carried out using AutoDock Vina, powerful software that gives ligands complete conformational flexibility while setting controlled flexibility on

16121880, 2026, 1, Downloaded from https://onlinelibrary.wiley.com/doi/10.1002/cbdv.202502169 by Bezm-I Alem Vakif University, Wiley Online Library on [07/01/2026]. See the Terms and Conditions (https://onlinelibrary.wiley.com/terms-and-conditions) on Wiley Online Library for rules of use; OA articles are governed by the applicable Creative Commons License

the receptors, improving the accuracy of binding predictions [22]. The Protein Data Bank (PDB) provided the three-dimensional crystal structure of BXO (PDB ID: 3nrz), which was identified as the receptor for system [21]. This structure, which was resolved at a high resolution of 1.8 Å, includes the critical cofactor-binding domains and is co-crystallised with the physiological substrate hypoxanthine, thus offering a precise characterisation of the active-site geometry [53]. The compounds selected for analysis were sourced from the PubChem database [54]. In the receptor preparation phase, the first phase requires the elimination of ligands, heteroatoms, co-crystallised solvents, and any extraneous molecules that are not directly related to the active site, as determined by AutoDock Vina (ADV). Subsequently, hydrogen atoms were infused into the macromolecule, resulting in a total of 21 602 hydrogens. This step was critical for accurately simulating protonation states, tautomeric forms, and hydrogen-bonding interactions within the binding site. A grid box structure was carefully defined to include the catalytic region of BXO after receptor optimisation. The box's dimensions were set to 20 × 22 × 22 Å, and its centre was at coordinates (x = 37.338, y = 19.791, z = 17.854). Using AutoDock Tools (ADT), the receptor was properly positioned in the grid centre with a 1 Å spacing. All other default parameters were used, with the sole modification being the output setting, which was limited to a single confirmation [55]. Various binding positions for every ligand were generated. The recurrence frequency of the predicted conformations and the lowest binding free energy values, measured in kcal/mol, were the two main criteria used to choose the ideal poses. Discovery Studio Visualiser was used to analyse and depict the final ligand-receptor complexes, allowing for a thorough analysis of the binding interactions.

2.11 | MD Simulation

MD simulation is a powerful computational technique that captures the temporal progression of atoms and molecules, offering detailed atomistic insights into their structural integrity, conformational variability, and dynamic properties [56]. Within the scope of drug discovery, MD simulations are crucial, as they facilitate the examination of ligand-protein interactions with high spatial and temporal resolution, thus contributing to the elucidation of binding stability [57]. The MD simulation of the current study was carried out to evaluate the stability and movement of the top-ranking complex ((+)-*trans* taxifolin-3nrz) obtained from molecular docking analysis. We have used CABS-flex 2.0 (https://biocomp.chem.uw.edu.pl/CABSflex2), an efficient platform designed for swift yet dependable simulations of protein structural dynamics [58]. This platform is specifically designed to generate the root mean square fluctuation (RMSF) profile, offering a comprehensive evaluation of the flexibility of individual amino acid residues within the binding pocket. Additionally, complementary dynamic analyses were conducted using the iMODS web server (https://imods.iqf.csic.es/). This platform was employed to extract additional dynamic descriptors, including deformability, *B*-factors, eigenvalues, and variance plots [59], which collectively facilitated a more profound comprehension of intrinsic motions and stability of the docked complexes.

3 | Results and Discussion

3.1 | XO Extraction

A yield of 6.43% of BXO was successfully obtained from 1.7 L of bovine milk. The enzyme's activity was confirmed by incubating the extract for 30 min under optimal conditions with a xanthine substrate ([xanthine] = 0.06 mg/mL). After incubation, a chromogenic reagent was added to the reaction mixture, and the absorbance at 505 nm was measured. The formation of a distinctive pink colour demonstrated evident catalytic activity, validating the extracted enzyme's activity.

3.2 | Phytochemical Composition Using LC–HRESIMS

The chemical characterisation of the *Z. lotus* seed ethyl acetate extract was performed using LC–HRESIMS, with the identified phytoconstituents listed in Tables 1 and 2 and illustrated in Figures 2 and 3. The extract showed a very complex chemical profile characterised by the presence of the fourteen phenolic compounds. Syringic acid, a derivative of sinapinic acid, was detected at high concentrations, with 16 240.00 µg/g extract for syringic acid and 3688.80 µg/g extract for sinapinic acid. These two compounds represented the most abundant phenolics in our extract and have also been previously reported in *Z. lotus* leaf and fruit extracts [60]. Computational studies of syringic acid-derived compounds revealed potent competitive XO inhibition in vitro, supported by molecular docking analyses highlighting key enzyme-ligand interactions [61]. Additionally, sinapinic acid has been demonstrated to inhibit XO both in vitro and in vivo, contributing to the normalisation of renal biomarkers and reducing inflammation [62]. In a recent comparative study of hydroxycinnamic acids, Dhammaraj et al. [63] reported that sinapinic acid exhibits moderate xanthine oxidase inhibitory activity ($IC_{50} \approx 117$ µM), with potency greater than caffeic acid [63]. Rutin, the third most abundant phenolic compound in *Z. lotus* seeds (1918.00 µg/g extract), is a bioflavonoid commonly found in plant-based foods and herbs. It is well known for its antioxidant properties [64] and multiple health-promoting effects, such as supporting cardiovascular health and reducing inflammation [65]. A recent study by Yu et al. [66] demonstrated that rutin and quercetin inhibit XO in vitro and significantly lower serum uric acid levels in animal models, supporting their potential as antigout agents [66]. Furthermore, Yahia et al. [67] confirmed the presence of rutin across different *Z. lotus* plant parts [67]. In addition, the seeds of *Z. lotus* contain significant amounts of apigenin-7-*O*-glucoside, salicylic acid, and luteolin-7-*O*-rutinoside, ranging between 214.24 and 240.46 µg/g extract. Salicylic acid, a simple phenolic acid, was also detected in the leaves of *Z. lotus* [68]. It was recognised for its weak XO inhibition, ranking among the least potent phenolic inhibitors [69]. Nonetheless, it is widely recognised for its anti-inflammatory and antibacterial agents [70]. Luteolin-7-*O*-glucoside and apigenin-7-*O*-glucoside were screened and identified as the candidate XO inhibitors [71], and their presence in the methanolic extracts of different *Ziziphus* species from Tunisia has also been reported [67]. However, the abundance of the luteolin-7-*O*-rutinoside in *Z. lotus* ethyl acetate extract, as well as its inhibitory activity against

16121880, 2026, 1, Downloaded from https://onlinelibrary.wiley.com/doi/10.1002/cbdv.202502169 by Bezm-I Alem Vakif University, Wiley Online Library on [07/01/2026]. See the Terms and Conditions (https://onlinelibrary.wiley.com/terms-and-conditions) on Wiley Online Library for rules of use; OA articles are governed by the applicable Creative Commons License

TABLE 1 | Qualitative and quantitative analysis of the phenolic compounds of the ethyl acetate fraction of *Ziziphus lotus* seeds by liquid chromatography–high-resolution electrospray ionisation mass spectrometry (LC–HRESIMS).

No	Phenolics	Molecular formula	µg/g extract	Relative uncertainty (%)
1	Salicylic acid	$C_7H_6O_3$	221.40	1.89
2	Caffeic acid	$C_9H_8O_4$	48.02	3.74
3	Syringic acid	$C_9H_{10}O_5$	16 240.00	3.71
4	Sinapinic acid	$C_{11}H_{12}O_5$	3688.80	3.57
5	Naringenin	$C_{15}H_{12}O_5$	26.00	4.20
6	Dihydrokaempferol	$C_{15}H_{12}O_6$	6.00	2.86
7	Quercetin	$C_{15}H_{10}O_7$	33.20	2.95
8	(+)-*trans* taxifolin	$C_{15}H_{12}O_7$	20.60	3.35
9	Myricetin	$C_{15}H_{10}O_8$	64.00	4.18
10	Apigenin 7-*O*-glucoside	$C_{21}H_{20}O_{10}$	240.46	3.59
11	Orientin	$C_{21}H_{20}O_{11}$	50.00	3.67
12	Naringin	$C_{27}H_{32}O_{14}$	62.00	4.20
13	Luteolin-7-*O*-rutinoside	$C_{27}H_{30}O_{15}$	214.24	3.06
14	Rutin	$C_{27}H_{30}O_{16}$	1918.00	3.07

TABLE 2 | Analytical standards used in liquid chromatography–high-resolution electrospray ionisation mass spectrometry (LC–HRESIMS) experiments.

Compound	Molecular formula	*m/z*	Ionization mode	Linear regression equation	LOD/LOQ	R^2	Recovery %	RSD
Salicylic acid	$C_7H_6O_3$	137.0244	Negatif	$y = 0.0361x + 0.00245$	0.01/0.03	0.9982	92.88	3.97
Caffeic acid	$C_9H_8O_4$	179.0350	Negatif	$y = 0.0304x + 0.00366$	0.08/0.27	0.9993	94.51	3.23
Syringic acid	$C_9H_{10}O_5$	197.0456	Negatif	$y = 0.0000831x + 0.000024$	0.1/0.3	0.9991	97.29	4.56
Sinapinic acid	$C_{11}H_{12}O_5$	223.0612	Negatif	$y = 0.0000543x - 0.0000251$	0.91–3.01	0.9989	97.61	4.67
Naringenin	$C_{15}H_{12}O_5$	271.0612	Negatif	$y = 0.0281x + 0.00182$	0.01/0.03	0.9995	86.65	1.52
Dihydrokaempferol	$C_{15}H_{12}O_6$	287.0561	Negatif	$y = 0.0756x + 0.0118$	0.01/0.03	0.995	95.37	3.75
Quercetin	$C_{15}H_{10}O_7$	447.0933	Negatif	$y = 0.0179x + 0.0003331$	0.01/0.03	0.999	97	4.76
(+)-*trans* taxifolin	$C_{15}H_{12}O_7$	303.0510	Negatif	$y = 0.0289x + 0.00537$	0.01/0.03	0.9978	91.66	3.26
Myricetin	$C_{15}H_{10}O_8$	317.0303	Negatif	$y = 0.0202x + 0.00165$	0.01/0.03	0.9993	100.1	4.17
Apigenin 7-*O*-glucoside	$C_{21}H_{20}O_{10}$	431.0984	Negatif	$y = 0.0246x + 0.00306$	0.01/0.03	0.9962	96.07	4.61
Orientin	$C_{21}H_{20}O_{11}$	447.0933	Negatif	$y = 0.00757x + 0.000347$	0.01/0.03	0.9993	96.22	4.16
Naringin	$C_{27}H_{32}O_{14}$	579.1719	Negatif	$y = 0.00576x - 0.000284$	0.01/0.03	0.9991	101.91	3.86
Luteolin-7-*O*-rutinoside	$C_{27}H_{30}O_{15}$	593.1512	Negatif	$y = 0.00879x + 0.000739$	0.01/0.03	0.9988	93.05	3.84
Rutin	$C_{27}H_{30}O_{16}$	609.1461	Negatif	$y = 0.00329x - 0.00005576$	0.01/0.03	0.999	96.97	4.12

the BXO, has not previously been demonstrated in the literature. For this reason, we employed in silico approaches to predict the potential of luteolin-7-*O*-rutinoside as an XOI. Other flavonoid glycosides were also detected in the *Z. lotus* extract, such as orientin (50 µg/g extract) and naringin (62 µg/g extract). Naringin has been identified in methanol-extracted leaves, seeds, and fruits of *Z. lotus* by Yahia et al. [67]. Although orientin is a common flavone glycoside in other plants, its occurrence in *Z. lotus* has not yet been confirmed in published studies. Nevertheless, both naringin and orientin and their related compounds have been evaluated for XOI, displaying only weak inhibitory activity [72, 73]. Flavonoid aglycones were also identified in the *Z. lotus* ethyl acetate extract, including quercetin (33.20 µg/g extract), myricetin (64 µg/g extract), and naringenin (26 µg/g extract). Both quercetin and myricetin showed strong activity against XO at low concentrations [74, 75], supporting the relevance of *Z. lotus* extract as promising antigout agents. Additionally, naringenin has been shown to inhibit XO in vitro and to suppress

16121880, 2026, 1, Downloaded from https://onlinelibrary.wiley.com/doi/10.1002/cbdv.202502169 by Bezm-I Alem Vakif University, Wiley Online Library on [07/01/2026]. See the Terms and Conditions (https://onlinelibrary.wiley.com/terms-and-conditions) on Wiley Online Library for rules of use; OA articles are governed by the applicable Creative Commons License

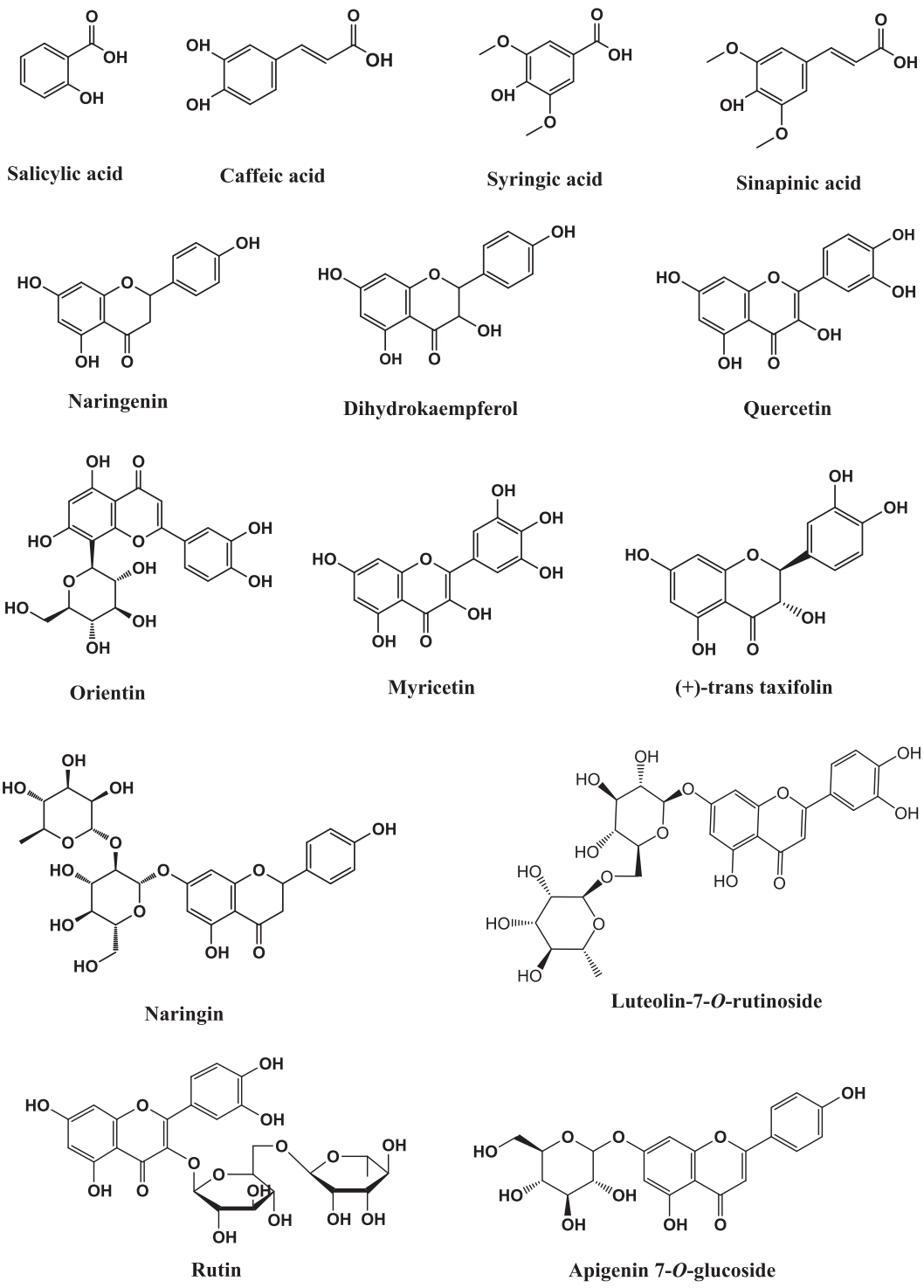

FIGURE 2 | Structural elucidation of compounds identified in the ethyl acetate extract of *Ziziphus lotus* seed.

XO activity in vivo in experimental hyperuricemia models. It was also identified as the strongest flavonoid XOI, contributing to the prevention and treatment of gout, related inflammatory disorders, and oxidative stress [76]. These compounds were detected in *Z. lotus* fruit extract, as reported by Bencheikh et al. [77], further reinforcing the abundance of these flavonoids within the *Ziziphus* genus. In the biosynthesis pathway, naringenin is converted into dihydrokaempferol by flavanone 3-hydroxylase (F3H), and dihydrokaempferol is then oxidised into kaempferol by flavonol synthase (FLS) [78] or converted to (+)-*trans* taxifolin (dihydroquercetin) by flavonoid-3′-hydroxylase (F3′H) [79]. In our extract, dihydrokaempferol and (+)-*trans* taxifolin were detected with 6 and 20.60 μg/g extract, respectively. Various studies demonstrate the efficacy of taxifolin in reducing uric acid, supporting its potential as hypouricemic and antigout agents [80]. Additionally, dihydrokaempferol possesses antioxidant and anti-inflammatory activity [81]. Despite the extensive phytochemical characterisation of flavonoids in *Z. lotus*, no earlier studies report

16121880, 2026, 1, Downloaded from https://onlinelibrary.wiley.com/doi/10.1002/cbdv.202502169 by Bezm-I Alem Vakif University, Wiley Online Library on [07/01/2026]. See the Terms and Conditions (https://onlinelibrary.wiley.com/terms-and-conditions) on Wiley Online Library for rules of use; OA articles are governed by the applicable Creative Commons License

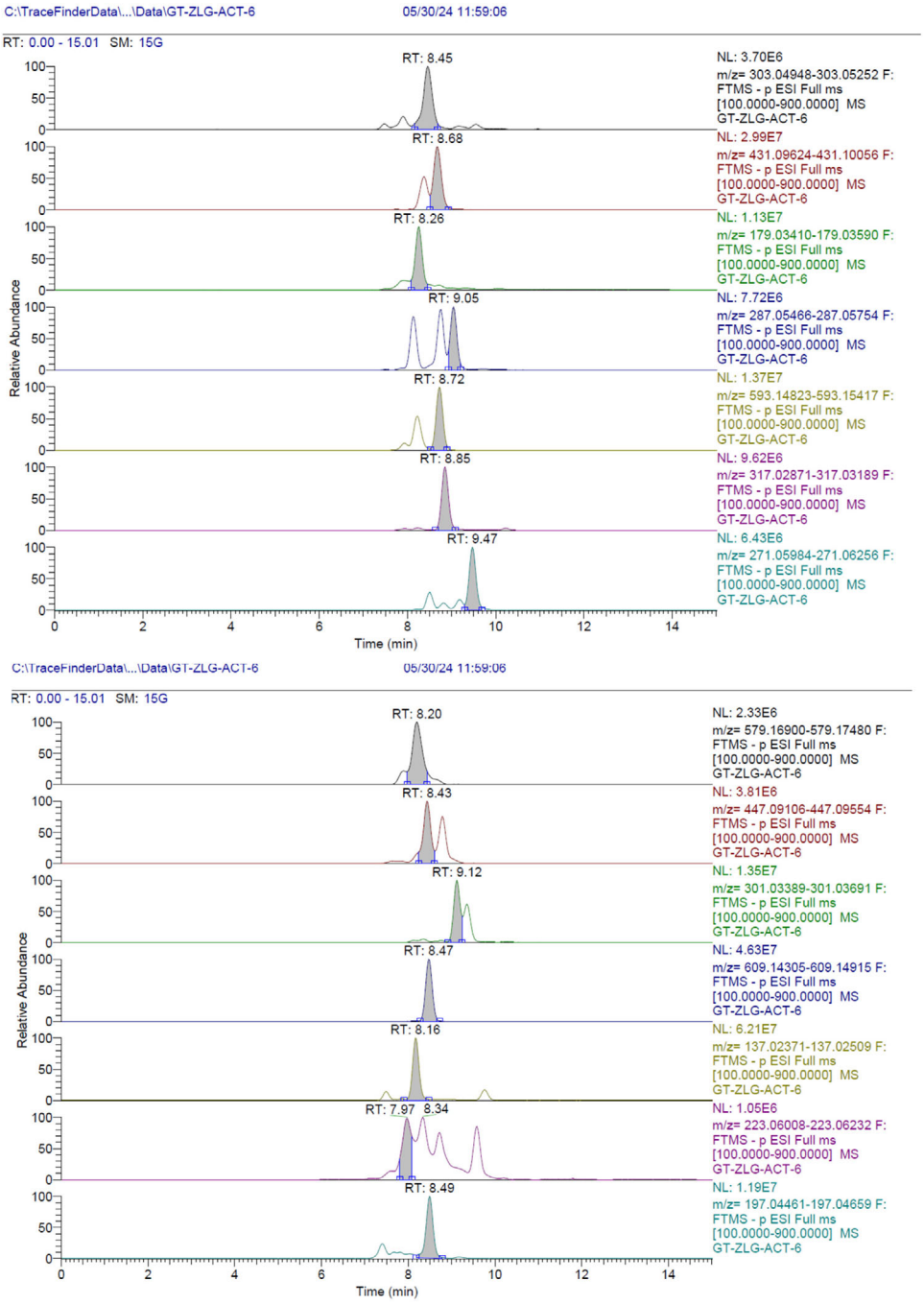

FIGURE 3 | LC–HRESIMS chromatograms of seed extract of *Ziziphus lotus*.

the presence of dihydrokaempferol or (+)-*trans* taxifolin in this plant. The seed extract was also enriched with caffeic acid at 48.02 μg/g extract, a well-known compound that has been shown to decrease serum uric acid levels in vivo and in vitro by regulating the mRNA transcription of the renal uric acid transporters [82]. Furthermore, it was reviewed as a major compound of the *Z. lotus* leaf part [83].

3.3 | XO Inhibition

The complex and incredibly varied chemical compositions of medicinal plants are known to control a broad range of biological processes. Various anatomical components, including seeds, leaves, stems, and flowers, have distinctive sets of bioactive ingredients that each contribute to the pharmacological potential of the plant [84]. The findings of our experiment on the inhibitory activity of BXO by the leaves and seeds of *Z. lotus* revealed a clear difference in degrees of potency between the two extracts, where the seed extract exhibited a stronger inhibition, with an IC_{50} of 40.63 ± 0.41 μg/mL, while the leaf extract displayed a comparatively weaker inhibitory effect, with an IC_{50} of 61.06 ± 1.15 μg/mL (Table 3). These results highlight the superior efficacy of seed extract over the leaf extract in suppressing BXO activity. Consequently suggesting that seeds provide a more promising source of bioactive chemicals for therapeutic utilisation. The observed

16121880, 2026, 1, Downloaded from https://onlinelibrary.wiley.com/doi/10.1002/cbdv.202502169 by Bezm-I Alem Vakif University, Wiley Online Library on [07/01/2026]. See the Terms and Conditions (https://onlinelibrary.wiley.com/terms-and-conditions) on Wiley Online Library for rules of use; OA articles are governed by the applicable Creative Commons License

TABLE 3 | Comparative IC_{50} values of *Ziziphus lotus* seed and leaf extracts in inhibiting bovine xanthine oxidase (BXO).

Extract	Seed	Leaf	Positive control (febuxostat)
IC_{50} (μg/mL)	40.63 ± 0.41	61.06 ± 1.15	0.0074 ± 0

disparity in inhibitory activity can be attributed to the distinct qualitative and quantitative phytochemical compositions of the extracts. Hydroxylated chemicals stand out among these components in terms of their mechanistic significance. The reduction of the molybdenum-hydroxyl catalytic system within the BXO active site becomes possible by their hydroxyl groups, acting as hydrogen donors. By obstructing the catalytic core, this interaction successfully inhibits enzymatic function and reduces the activity of the enzyme [22]. To the best of our understanding, *Z. lotus* has not previously been investigated for its potential to inhibit XO. In contrast, a well-studied member of the Rhamnaceae family, *Rhamnus alaternus*, has consistently exhibited relatively weak XO inhibition, with reported IC_{50} values typically exceeding 65 μg/mL [85]. Notably, when considered within the broader phytochemical framework of the Rhamnaceae family, *Z. lotus* appears to display markedly stronger XO inhibitory activity, highlighting its promising potential as a novel source of natural XO inhibitors.

3.4 | PASS Study

Through the use of a web server to estimate the predicted biological activities (PBA) of the selected compounds from *Z. lotus* seeds, the findings indicated that both compounds were forecasted to inhibit XO and contribute to gout treatment. For (+)-*trans* taxifolin, it appears with a relatively high PBA value of 1203 and a greater Pa value range of 0.825 for gout treatment, indicating its significant potential for effectively managing gout. However, its Pa of XOI is more moderate, achieving a value of 0.462. The second compound, luteolin-7-*O*-rutinoside, exhibited 787 PBA, with an effective value of Pa = 0.597 for blocking XO activity.

3.5 | ADMET and DL Evaluation

3.5.1 | ADMET Screening

Pharmacokinetic parameters calculated by running the servers (Table 4) indicate that none of the investigated compounds showed effective permeability across Caco-2 cell monolayers, since all values fell below the predetermined threshold. In addition, human intestinal absorption was classified as low. Importantly, no inhibition was detected for P-glycoprotein in any compound. Regarding the distribution profile, both predicted compounds failed to cross the blood–brain barrier (BBB) or penetrate MDCK cells, with scores falling below the norm. Furthermore, they displayed pronounced plasma protein-binding affinities. Both of the compounds exhibited inhibitory action against cytochrome P450 isoforms CYP3A4, CYP2C19, and CYP2C9, according to the metabolic profile; however, neither compound inhibited or acted as a substrate for CYP2D6. Regarding the excretion profile, both compounds exhibited relatively short half-lives, indicating minimal time required for metabolic mechanisms, with clearance rates consistently classified as low to moderate. Toxicological assessments produced highly favourable outcomes; there was no sign of human hepatotoxicity, nephrotoxicity, or hematotoxicity in any of the chemicals that were evaluated.

3.5.2 | POM Analysis

The Osiris calculations revealed distinct pharmacokinetic and physicochemical profiles for the investigated compounds (depicted in Table 5). The examination of theoretical toxicity risks indicated that both compounds are non-mutagenic, non-tumorigenic, and present no reproductive risks, along with no irritant effects. The hydrophilicity character of each compound has been quantified by the cLog *P* value. It has been demonstrated that the absorption or permeation is significantly influenced by the cLog *P* value. Thus, when the cLog *P* exceeds 5, the rate of absorption or permeation decreases [44]. Based on this, (+)-*trans* taxifolin exhibited favourable lipophilicity (cLog $P = 0.96$). The solubility of a compound in water plays a crucial role in determining its absorption and distribution properties. It is estimated that over 80% of the pharmaceuticals available in the market possess a cLog *S* value exceeding −4 [86]. In the case of (+)-*trans* taxifolin, it has moderate solubility. Additionally, lipophilicity (cLog *P*) and polar surface area (TPSA) are two crucial properties for predicting the oral bioavailability of drug molecules. The polar surface area (TPSA) is determined by the surface areas occupied by oxygen and nitrogen atoms, as well as by hydrogen atoms that are bonded to them and/or to metal atoms. It has been demonstrated to be an excellent descriptor for characterising drug absorption, including intestinal absorption, bioavailability, Caco-2 permeability, and penetration through the BBB [87]. Compounds with TPSA values around 160 or higher are anticipated to show poor intestinal absorption. In the case of (+)-*trans* taxifolin, the TPSA falls within the normal range, indicating sufficient oral absorption and membrane permeability. The software also provides the DL and DS of the compound; (+)-*trans* taxifolin exhibits a high DL index of 2.03 and a DS of 0.87, underscoring its strong potential as a drug-like candidate that adheres to Lipinski's rule of five. In contrast, luteolin-7-*O*-rutinoside possesses a high MW exceeding 500 Da, which is further influenced by its low lipophilicity (cLog $P = -0.91$) and a very high TPSA value. These characteristics may impede intestinal absorption and permeability, potentially resulting in poor oral bioavailability. This situation elucidates its relatively lower DS of 0.59, despite a higher DL value of 3.66, which reflects the presence of multiple pharmacophoric features. For Molinspiration calculations (Table 6), (+)-*trans* taxifolin yielded results consistent with Osiris data, where cLog *P* was 0.71, TPSA was 127.4 $Å^2$ (below the 160 threshold), MW was 304.3 Da (below 500), with H-bond acceptors (nON) at 7, donors (nOHNH) at 5, one rotatable bond, and no Lipinski violations. These parameters adhere to Lipinski's guidelines, indicating favourable oral DL. Conversely, luteolin-7-*O*-rutinoside is predicted to exhibit poor passive diffusion and low oral bioavailability, with a cLog *P* of −0.51, a TPSA of 249.2 $Å^2$, and a MW of 594.5 Da. It has 15 H-bond

16121880, 2026, 1, Downloaded from https://onlinelibrary.wiley.com/doi/10.1002/cbdv.202502169 by Bezm-I Alem Vakif University, Wiley Online Library on [07/01/2026]. See the Terms and Conditions (https://onlinelibrary.wiley.com/terms-and-conditions) on Wiley Online Library for rules of use; OA articles are governed by the applicable Creative Commons License

TABLE 4 | Evaluation of ADMET properties in ligands.

Pharmacokinetics	(+)-*trans* taxifolin	Luteolin-7-*O*-rutinoside
	Absorption	
Caco-2 cell permeability (nm/s)	3.42	6.41
Human intestinal absorption (HIA %)	60.16	6.28
P-glycoprotein inhibition	Non	Non
Buffer solubility (mg/L)	655.53	53.08
	Distribution	
Blood–brain barrier penetration (*C*.brain/*C*.blood)	0.16	0.02
MDCK cell permeability (nm/s)	9.56	0.05
Plasma protein binding (%)	95.16	54.83
Skin permeability	−4.42	−4.56
	Metabolism	
Cytochrome P450 2D6 inhibition	Non	Non
Cytochrome P450 2D6 substrate	Non	Non
Cytochrome P450 3A4 inhibition	Inhibitor	Inhibitor
Cytochrome P450 3A4 substrate	Weakly	Weakly
Cytochrome P450 2C19 inhibition	Inhibitor	Inhibitor
Cytochrome P450 2C9 inhibition	Inhibitor	Inhibitor
	Excretion	
Clearance	12.28	1.54
$T_{1/2}$	0.75	4.87
	Toxicity	
Carcinogenicity	0.24	0.02
Hepatotoxicity	0.49	0.25
Nephrotoxicity	0.12	0.03
Hematotoxicity	0.07	0.007

TABLE 5 | In silico screening of toxicity risks and drug-score using the Osiris platform.

Compound	MW	Toxicity risks				Physicochemical properties				
		MUT	TUM	IRRI	REP	cLog *P*	Sol	TPSA	DL	DS
(+)-*trans* Taxifolin	304.2	Not toxic	Not toxic	Not toxic	Not toxic	0.96	−1.94	127.4	2.03	0.87
Luteolin-7-*O*-rutinoside	594.5	Not toxic	Not toxic	Not toxic	Not toxic	−0.91	−2.65	245.2	3.66	0.59

Abbreviations: DL, drug-likeness; DS, drug score; IRRI, irritant; MUT, mutagenic; MW, molecular weight; REP, reproductive effective; Sol, solubility; TPSA, topological polar surface area; TUM, tumorigenic.

acceptors, 9 donors, 6 rotatable bonds, and 3 Lipinski violations, all exceeding acceptable limits. Collectively, this underscores (+)-*trans* taxifolin as the more promising drug candidate in comparison to luteolin-7-*O*-rutinoside.

3.6 | Pharmacophore Modelling

The pharmacophore modelling outcomes for the ligands revealed distinct spatial distributions of chemical features that contribute to their XO inhibition, as shown in Figure 4. The aromatic rings of both ligands exhibited notable aromatic regions in purple, which are associated with π–π stacking or hydrophobic interactions within the enzyme's active site. Additionally, this ring displayed hydrophobic centres (in green), along with the hydrophobic characteristics noted for the methyl group of luteolin-7-*O*-rutinoside, which further enhanced these nonpolar interactions. Furthermore, multiple hydrogen bond acceptor and donor sites (orange and grey, respectively, in Figure 4.) were identified, suggesting the potential for the formation of stable hydrogen bonds that

16121880, 2026, 1, Downloaded from https://onlinelibrary.wiley.com/doi/10.1002/cbdv.202502169 by Bezm-I Alem Vakif University, Wiley Online Library on [07/01/2026]. See the Terms and Conditions (https://onlinelibrary.wiley.com/terms-and-conditions) on Wiley Online Library for rules of use; OA articles are governed by the applicable Creative Commons License

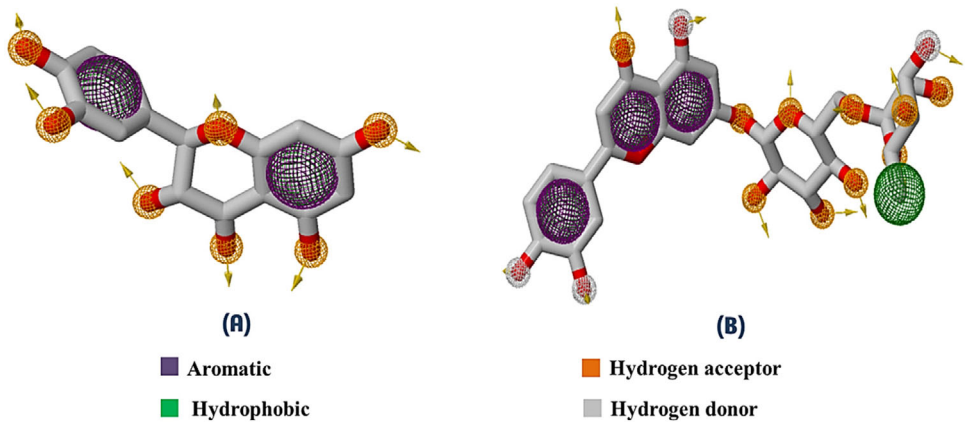

FIGURE 4 | 3D pharmacophore models of (+)-*trans* taxifolin (A) and luteolin-7-*O*-rutinoside (B) illustrating the key chemical features involved in xanthine oxidase inhibition.

TABLE 6 | Computational prediction of drug-likeness parameters via Molinspiration analysis.

Parameters	(+)-*trans* taxifolin	Luteolin-7-*O*-rutinoside
cLog *P*	0.71	−0.51
TPSA	127.44	249.20
MW	304.25	594.52
n-atoms	22	42
nON	7	15
nOHNH	5	9
n-violations	0	3
n-rotb	1	6
Volume	246.32	488.05

Abbreviations: MW, molecular weight; TPSA, topological polar surface area.

enhance binding stability, with luteolin-7-*O*-rutinoside exhibiting the highest number of such interactions, indicating its stronger and multi-point interactions with the enzyme.

3.7 | Molecular Docking

The inhibitory activity of newly selected compounds was elucidated through their incorporation within the active site cavity of BXO (PDB ID: 3nrz). After docking, the ligands formed a complex network of interactions with catalytically important amino acid residues, including hydrophobic contacts, hydrogen bonds and other non-covalent interactions. These interactions justified the compounds' potential as powerful inhibitors by helping to damage the catalytic mechanism of the enzyme in addition to carefully anchoring them within the binding region.

(+)-*trans* taxifolin, also known as dihydroquercetin, is a flavonoid that falls under the flavanonol subclass. The presence of functional groups, such as hydroxyl and carbonyl groups substituted on various inhibitor rings, participates in the formation of numerous hydrogen bonds. In cycle A, hydroxyl groups form three hydrogen bonds with Thr1083 (3.11 Å), Val1259 (2.8 Å), and Gly1260 (3.13 Å). Meanwhile, the cycle B hydroxyl group in position 3′ interacts with the two catalytic amino acids Glu1261 and Ala1079, resulting in the formation of two conventional hydrogen bonds of 2.58 and 2.94 Å, respectively. Furthermore, the substitution of a carbonyl group on cycle C results in the establishment of a supplementary hydrogen bond with Gln1040, characterised by an interatomic distance of 2.6 Å. Beyond these polar contacts, a single hydrophobic interaction of the π-alkyl type was observed with Arg912, further contributing to the stabilisation of the ligand-protein complex. The finding of this interaction explains the significant affinity of the ligand towards BXO (PDB ID: 3nrz). These interactions, when considered together, elucidate the robust binding affinity of (+)-*trans* taxifolin for BXO (PDB ID: 3nrz), as demonstrated by its favourable docking score of −7.5 kcal/mol, underscoring its potential as a powerful enzyme inhibitor.

Luteolin-7-*O*-rutinoside is a flavonoid glycoside where the flavonoid luteolin is linked at position 7 to a disaccharide rutinose, which consists of a glucose and a rhamnose unit [88]. The analysis of the molecular docking data revealed that luteolin-7-*O*-rutinoside docked within the active site, achieving a binding energy of −6.82 kcal/mol. Its structure formed a tunnel-like structure. The substitution of rutinose on the flavonoid significantly enhances its ability to form crucial hydrogen interactions. A total of 10 hydrogen bonds were observed between the ligand and the amino acids Gln1194 (2.37 Å), Gly1260 (2.94 Å), Thr1083 (3.08 Å), Glu1261 (3 Å), Met1038 (2.75 Å), Ser1080 (2.42 Å), Gly799 (2.68 Å), Arg880 (2.92 Å), Gln767 (2.68 Å), and Thr1010 (3.35 Å), with the hydroxyl group being the primary contributor. This highlights the essential role of the sugar moiety in mediating the inhibitory activities of this ligand. The benzene rings of the ligand were orientated to promote π-alkyl and π-sigma interaction types with the hydrophobic amino acid residues Val1011 (5.09 Å), Leu1014 (4.63 Å), Leu873 (3.27 Å), Ala910 (5.48 Å), Ala1078 (4.25; 4.89 Å), and Ala1079 (3.93; 4.31 Å). However, the aromatic rings of Phe914 and Phe1009 contribute to π–π-stacked and π–π-T-shaped interactions with distances of 3.54 and 4.79 Å, respectively. While a single alkyl interaction with Leu1042 is observed at a distance of 4.11 Å, further stabilising the ligand-protein complex.

A comparative examination of the binding characteristics profiles of our chosen inhibitors and the standard reference drug,

16121880, 2026, 1, Downloaded from https://onlinelibrary.wiley.com/doi/10.1002/cbdv.202502169 by Bezm-I Alem Vakif University, Wiley Online Library on [07/01/2026]. See the Terms and Conditions (https://onlinelibrary.wiley.com/terms-and-conditions) on Wiley Online Library for rules of use; OA articles are governed by the applicable Creative Commons License

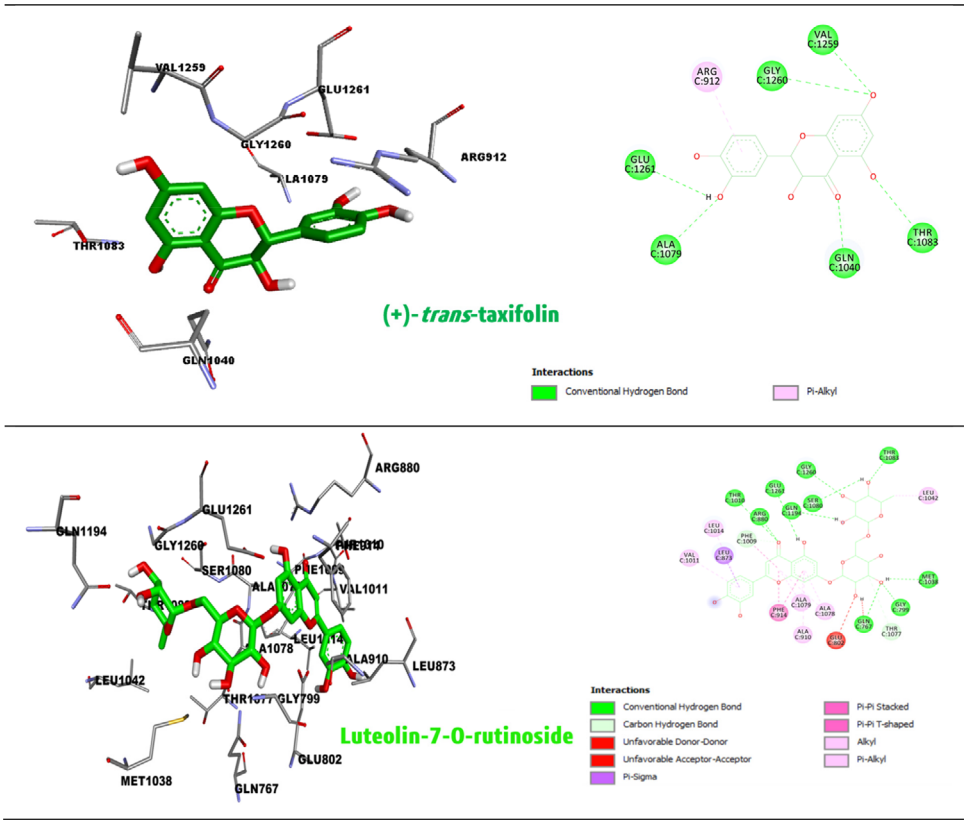

FIGURE 5 | The optimal poses of selected inhibitors within the active site of bovine xanthine oxidase (PDB ID: 3nrz).

febuxostat, which is complexed with BXO (PDB ID: 3nrz), reveals that (+)-*trans* taxifolin binds more strongly, reflected in its lower binding energy score. The distinctive patterns of hydrogen bonding that were seen are primarily responsible for this stronger interaction. The enzyme-ligand combination is more stable because our inhibitors form a far higher number of conventional hydrogen bonds than febuxostat, which only forms a small number of hydrogen bonds in the active site. The abundance of hydroxyl substituents and the associated sugar moieties, which easily interact with the hydroxyl, carbonyl, and amine groups of important amino acid residues in the catalytic pocket, are the main source of increased binding strength of flavonoid-based inhibitors. Furthermore, both the inhibitors and febuxostat exhibit similar types of interactions. Overall, luteolin-7-*O*-rutinoside stands out due to the additional presence of π–π-stacked and π–π-T-shaped interactions. These aromatic interactions considerably bolster the structural integrity of the ligand-target complex, contributing to a more stable ligand-target complex. A summary of the binding energy comparisons and full interaction profiles is depicted in Figure 5 and Table 7.

3.8 | Molecular Dynamic Simulation

To gain deeper validation of ligand-enzyme interactions, we proceeded to MD simulations after performing a molecular docking study of previously unidentified phytoconstituents extracted from *Z. lotus* seed extract. The detailed analysis focused on the top-ranking complex, (+)-*trans* taxifolin, bound to 3nrz.

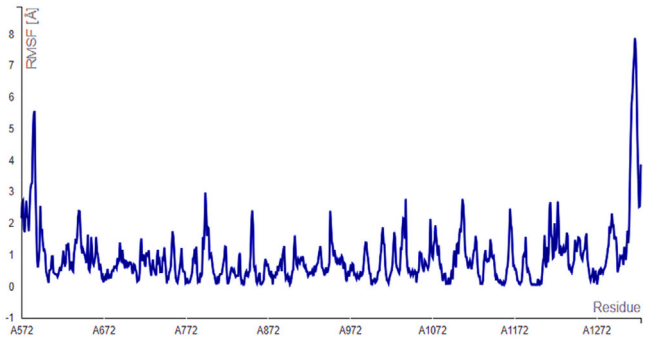

FIGURE 6 | RMSF curve of the (+)-*trans* taxifolin-3nrz complex generated using the CABS-flex server. RMSF, root mean square fluctuation.

3.8.1 | CABS-Flex Dynamic Simulation

The CABS-flex simulation generated an RMSF profile once the docked protein-ligand complex was submitted. This profile quantitatively describes the dynamic flexibility of individual residues during a trajectory of 10 ns (Figure 6). Greater flexibility is represented by elevated RMSF values, while lower values signify structural stiffness and stability. RMSF values serve as an indicator of local conformational mobility. The result revealed that residue 1198 exhibited the least fluctuation (0.046 Å), underscoring its exceptional structural stability, whereas residue 1319 displayed the highest RMSF of 7.875 Å, suggesting localised flexibility at that site. Interestingly, most of the protein-ligand complex's residues had RMSF values below 3 Å, which is

16121880, 2026, 1, Downloaded from https://onlinelibrary.wiley.com/doi/10.1002/cbdv.202502169 by Bezm-I Alem Vakif University, Wiley Online Library on [07/01/2026]. See the Terms and Conditions (https://onlinelibrary.wiley.com/terms-and-conditions) on Wiley Online Library for rules of use; OA articles are governed by the applicable Creative Commons License

TABLE 7 | The molecular docking outcomes of bovine xanthine oxidase (BXO) (Protein Data Bank [PDB] ID: 3nrz) with ligands.

Ligands	Energy (kcal/mol)	Repeating ratio %	Closest residues	Interactions type	Hydrogen bonds	Length (Å)
(+)-*trans* taxifolin	−7.5	90	Arg912	π-Alkyl	Glu1261 Ala1079 Gly1260 Val1259 Gln1040 Thr1083	>2.5
Luteolin-7-*O*-rutinoside	−6.82	50	Val1011, Leu1014, Phe1009, Ala1079, Leu1042, Ala1078, Ala910, Glu802, Leu873, Thr1077, Phe914	Alkyl π-Alkyl π–π-Stacked π–π-T-Shaped π-Sigma	Gln1194 Gly1260 Thr1083 Glu1261 Met1038 Gly799 Ser1080 Arg880 Thr1010 Gln767	>2.25
Febuxostat	−7.08	60	Gln1040, Phe798, Ala910, Phe914, Ala1078, Leu1042	Alkyl π-Alkyl π-Sigma	Lys1045	2.81 3.08

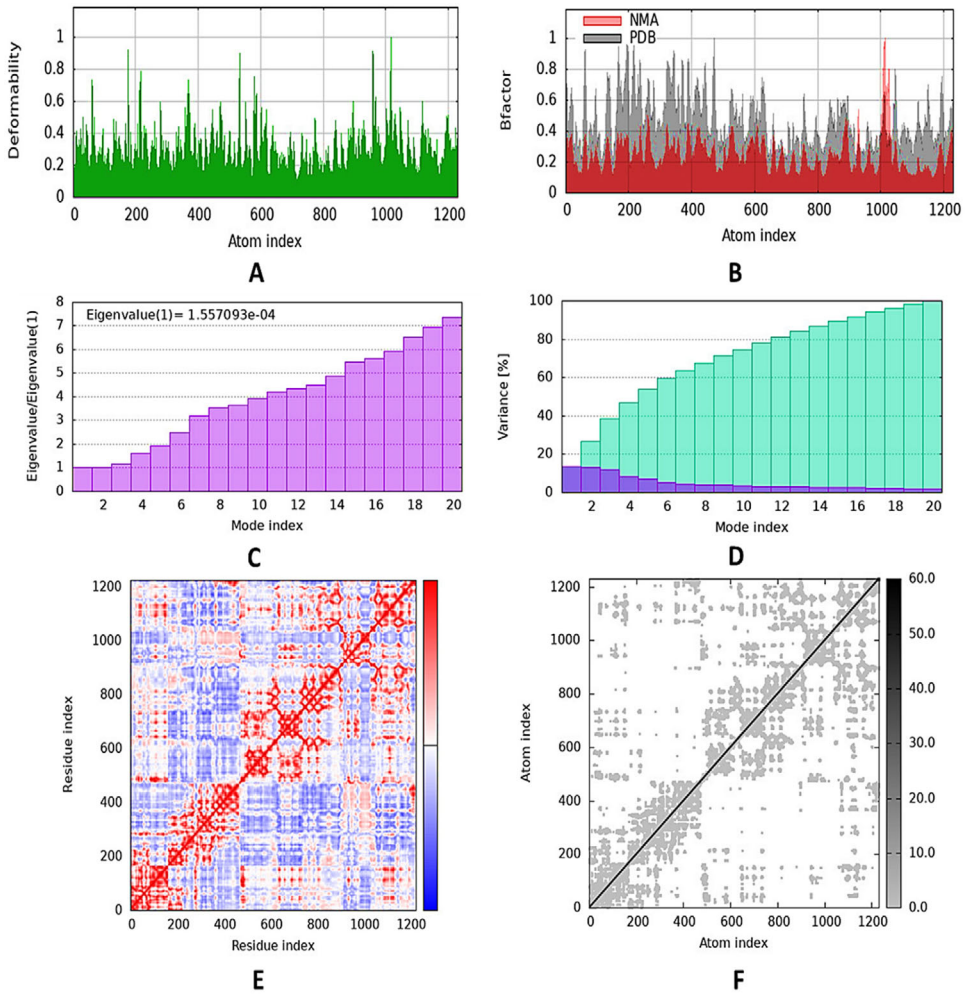

FIGURE 7 | MD simulation outcomes of the (+)-*trans* taxifolin-3nrz complex using the iMODS server. (A) deformability characteristics, (B) B-factor graphs, (C) the eigenvalue, (D) variance, (E) correlation matrix, (F) elastic network. NMA, normal mode analysis; PDB, Protein Data Bank.

16121880, 2026, 1, Downloaded from https://onlinelibrary.wiley.com/doi/10.1002/cbdv.202502169 by Bezm-I Alem Vakif University, Wiley Online Library on [07/01/2026]. See the Terms and Conditions (https://onlinelibrary.wiley.com/terms-and-conditions) on Wiley Online Library for rules of use; OA articles are governed by the applicable Creative Commons License

frequently linked to stable conformational behaviour. Specifically, we found that all seven key residues involved in crucial hydrogen and hydrophobic interactions within the active site displayed low RMSF values. In particular, Arg912 (0.87 Å), Glu1261 (0.92 Å), Ala1079 (0.97 Å), Gly1260 (1.66 Å), Val1259 (1.54 Å), Thr1083 (0.64 Å), and Gln1040 (2.76 Å) exhibited minimal fluctuations during the simulation. These low RMSF values indicate that the residues maintain a stable conformation, thereby reinforcing the stable incorporation of the ligand within the active site. A simulation lasting 10 ns is sufficient for this objective, as it allows us to determine whether the hydrogen bonds and hydrophobic interactions identified through docking remain stable in a dynamic and aqueous environment. The findings confirmed that the essential interactions are preserved, thereby validating the docking predictions. We recognise that longer simulations would be required to investigate the entire conformational space; however, this falls outside the purview of this study, which aims at a swift validation of the optimal docking complexes.

3.8.2 | IMODS Dynamics Simulation

The MD simulation result obtained from the iMOD server, specifically through normal mode analysis (NMA), provided substantial data on the dynamic stability of the docked protein-ligand complex, as illustrated in Figure 7. Regions with greater peaks are more structurally flexible. Conversely, regions with few fluctuations imply stability and structural stiffness. According to our complex curve, the majority of residues had low deformability values (<0.5), demonstrating the complex's structural stability. The calculated eigenvalue for the complex was 1.557093e − 04, a relatively low value that indicates that minimal energy is needed to induce conformational changes. This low eigenvalue suggests that the docked conformation may support minor structural modifications while preserving overall stability.

4 | Conclusion

By integrating comprehensive phytochemical characterisation with advanced in silico modelling, this study represents the first comprehensive exploration of *Z. lotus* as potential anti-gout therapeutics. The inhibitory capacity of its extract against bovine XO was validated through in vitro assays and is strongly corroborated by the phytochemical profile of the potent extract, which harbours key XOIs within the plant extract. Among the identified metabolites, (+)-*trans* taxifolin and luteolin-7-*O*-rutinoside represent novel and particularly compelling phytochemicals. Their identification highlights the necessity of advanced computational validation to further elucidate their inhibitory mechanisms and to confirm their capacity as drug-like candidates, which presently indicates a lack of human toxicity. Collectively, these findings establish a critical foundation for the targeted isolation of active constituents from *Z. lotus* and emphasise the importance of future in vivo and clinical studies to validate its therapeutic efficacy in gout management.

Funding

The authors have nothing to report.

Ethics Statement

This study did not require ethical approval, as it does not involve human or animal subjects.

Consent

The authors have nothing to report.

Conflicts of Interest

The authors declare no conflicts of interest.

Data Availability Statement

All data generated or analysed during this study are included in this manuscript. No additional datasets were generated or used.

References

1. L. Ait Abderrahim, K. Taïbi, and C. Ait Abderrahim, "Assessment of the Antimicrobial and Antioxidant Activities of *Ziziphus lotus* and *Peganum harmala*," *Iranian Journal of Science and Technology, Transactions A: Science* 43 (2019): 409–414, https://doi.org/10.1007/s40995-017-0411-x.

2. N. Bencheikh, M. Bouhrim, I. A. Merrouni, et al., "Antihyperlipidemic and Antioxidant Activities of Flavonoid-Rich Extract of *Ziziphus lotus* (L.) Lam. Fruits," *Applied Sciences* 11 (2021): 7788, https://doi.org/10.3390/app11177788.

3. S. Abdoul-Azize, "Potential Benefits of Jujube (*Zizyphus lotus* L.) Bioactive Compounds for Nutrition and Health," *Nutrition and Metabolism* 2016 (2016): 2867470.

4. F. Berkani, M. L. Serralheiro, F. Dahmoune, et al., "*Ziziphus lotus* (L.) Lam. Plant Treatment by Ultrasounds and Microwaves to Improve Antioxidants Yield and Quality: An Overview," *North African Journal of Food and Nutrition Research* 5 (2021): 53–68, https://doi.org/10.51745/najfnr.5.12.53-68.

5. S. Saad, I. Dávila, F. Mannai, J. Labidi, and Y. Moussaoui, "Effect of the Autohydrolysis Treatment on the Integral Revalorisation of *Ziziphus lotus*," *Biomass Conversion and Biorefinery* 14 (2024): 1413–1425, https://doi.org/10.1007/s13399-022-02457-6.

6. A. Alsayari and S. Wahab, "Genus *Ziziphus* for the Treatment of Chronic Inflammatory Diseases," *Saudi Journal of Biological Sciences* 28 (2021): 6897–6914, https://doi.org/10.1016/j.sjbs.2021.07.076.

7. N. E. Yakoubi, Z. N. E. Ansari, M. Ennami, et al., "Assessment of Phytochemical, Antioxidant and Antibacterial Properties of *Ziziphus lotus* Leaves Extracts," *Multidisciplinary Science Journal* 7 (2025): 2025050, https://doi.org/10.31893/multiscience.2025050.

8. W. Borgi, M. C. Recio, J. L. Ríos, and N. Chouchane, "Anti-Inflammatory and Analgesic Activities of Flavonoid and Saponin Fractions From *Zizyphus lotus* (L.) Lam," *South African Journal of Botany* 74 (2008): 320–324, https://doi.org/10.1016/j.sajb.2008.01.009.

9. N. Bencheikh, M. Bouhrim, I. A. Merrouni, et al., "Antihyperlipidemic and Antioxidant Activities of Flavonoid-Rich Extract of *Ziziphus lotus* (L.) Lam. Fruits," *Applied Sciences* 11 (2021): 7788, https://doi.org/10.3390/app11177788.

10. S. Ouldchikh, A. TirTouil, and B. Meddah, "*Zizyphus lotus* (L.) Extracts as Prebiotics in the Aggregation and Adhesion of Probiotic and Inhibition of Pathologic Bacteria From Patients With Colorectal Cancer," *International Journal of Food Studies* 9 (2020): 160–177.

11. I. Marmouzi, M. Kharbach, M. El Jemli, et al., "Antidiabetic, Dermatoprotective, Antioxidant and Chemical Functionalities in *Zizyphus lotus* Leaves and Fruits," *Industrial Crops and Products* 132 (2019): 134–139, https://doi.org/10.1016/j.indcrop.2019.02.007.

16121880, 2026, 1, Downloaded from https://onlinelibrary.wiley.com/doi/10.1002/cbdv.202502169 by Bezm-I Alem Vakif University, Wiley Online Library on [07/01/2026]. See the Terms and Conditions (https://onlinelibrary.wiley.com/terms-and-conditions) on Wiley Online Library for rules of use; OA articles are governed by the applicable Creative Commons License

12. S. Bendiar, O. El Faqer, N. Benjelloun, et al., "Immunosuppressive Effect of *Ziziphus lotus* L.(Desf.) Fruit's Extract on Neutrophil Bactericidal Activity and on In Vivo Humoral Immune Response in Mice," *Biomedical and Pharmacology Journal* 15 (2022): 2331–2341, https://doi.org/10.13005/bpj/2572.

13. E. El Maaiden, "Phenolic Profiling and Inhibitory Activities of Cholinesterase and β-Amyloid Aggregation in *Ziziphus* Species Fruit Fractions," *Journal of Food Biochemistry* 2024 (2024): 4695284, https://doi.org/10.1155/jfbc/4695284.

14. G. Ragab, M. Elshahaly, and T. Bardin, "Gout: An Old Disease in New Perspective—A Review," *Journal of Advanced Research* 8 (2017): 495–511, https://doi.org/10.1016/j.jare.2017.04.008.

15. S. S. P. Mohamed Isa, A. Ablat, and J. Mohamad, "The Antioxidant and Xanthine Oxidase Inhibitory Activity of *Plumeria rubra* Flowers," *Molecules (Basel, Switzerland)* 23 (2018): 400, https://doi.org/10.3390/molecules23020400.

16. C. Y. Huang, Y. Y. Chang, S. T. Chang, and H. T. Chang, "Xanthine Oxidase Inhibitory Activity and Chemical Composition of *Pistacia chinensis* Leaf Essential Oil," *Pharmaceutics* 14 (2022): 1982.

17. I. E. Orhan and F. S. Deniz, "Natural Products and Extracts as Xantine Oxidase Inhibitors-A Hope for Gout Disease?," *Current Pharmaceutical Design* 27 (2021): 143–158, https://doi.org/10.2174/1381612826666200728144605.

18. S. E. Conneely, S. L. Cooper, and R. E. Rau, "Use of Allopurinol to Mitigate 6-Mercaptopurine Associated Gastrointestinal Toxicity in Acute Lymphoblastic Leukemia," *Frontiers in Oncology* 10 (2020): 1129, https://doi.org/10.3389/fonc.2020.01129.

19. P. L. Owen and T. Johns, "Xanthine Oxidase Inhibitory Activity of Northeastern North American Plant Remedies Used for Gout," *Journal of Ethnopharmacology* 64 (1999): 149–160, https://doi.org/10.1016/S0378-8741(98)00119-6.

20. A. Baghiani, R. Harrison, and M. Benboubetra, "Purification and Partial Characterisation of Camel Milk Xanthine Oxidoreductase," *Archives of Physiology and Biochemistry* 111 (2003): 407–414, https://doi.org/10.3109/13813450312331342265.

21. A. Linani, K. Benarous, L. Bou-Salah, and M. Yousfi, "Hispidin, Harmaline, and Harmine as Potent Inhibitors of Bovine Xanthine Oxidase: Gout Treatment, In Vitro, ADMET Prediction, and SAR Studies," *Bioorganic Chemistry* 112 (2021): 104937, https://doi.org/10.1016/j.bioorg.2021.104937.

22. A. Linani, T. Serseg, K. Benarous, et al., "*Cupressus sempervirens* L. Flavonoids as Potent Inhibitors to Xanthine Oxidase: In Vitro, Molecular Docking, ADMET and PASS Studies," *Journal of Biomolecular Structure & Dynamics* 41 (2023): 7055–7068, https://doi.org/10.1080/07391102.2022.2114943.

23. L. Bou-Salah, K. Benarous, A. Linani, I. Bombarda, and M. Yousfi, "In Vitro and In Silico Inhibition Studies of Five Essential Oils on Both Enzymes Human and Bovine Xanthine Oxidase," *Industrial Crops and Products* 143 (2020): 111949, https://doi.org/10.1016/j.indcrop.2019.111949.

24. K. Benarous, L. Bou-Salah, A. Linani, M. Yousfi, I. Kostova, and L. Saso, "Lanthanide (III) Complexes of Bis-Coumarins as Strong Inhibitors of Bovine Xanthine Oxidase—Molecular Docking and SAR Studies," *Journal of Biomolecular Structure & Dynamics* 40 (2022): 2733–2739, https://doi.org/10.1080/07391102.2020.1842247.

25. H. İ. Öztürk, "The Effect of Different Lyophilisation Pressures on the Microbiological Stability, Physicochemical, Microstructural, and Sensorial Properties of Yoghurt Powders," *International Dairy Journal* 129 (2022): 105347.

26. E. Erol, "Quantitative Analysis of Bioaccessible Phenolic Compounds in Aegean Bee Bread Using LC–HRMS Coupled With a Human Digestive System Model," *Chemistry and Biodiversity* 21 (2024): e202301497, https://doi.org/10.1002/cbdv.202301497.

27. H. Bouakkaz, E. Erol, K. Benarous, et al., "Determining the Optimal Antioxidant Strategy: A Comparative Analysis of Extractionmethods in *Cistus villosus* L. Extracts Revealed by LC–HRMS and Computational Modeling," *Turkish Journal of Biology* 49 (2025): 1–27, https://doi.org/10.55730/1300-0152.2720.

28. N. Cherrada, A. E. Chemsa, E. Erol, et al., "Phytochemical Profiling of Salsola tetragona Delile by LC-HR/MS and Investigation of the Antioxidant, Anti-Inflammatory, Cytotoxic, Antibacterial and Anti-SARS-CoV-2 Activities," *Saudi Pharmaceutical Journal* 31 (2023): 101731.

29. G. Tel, B. Doğan, E. Erol, et al., "Determination of Antioxidant, Anticholinesterase, Tyrosinase Inhibitory Activities and Fatty Acid Profiles of 10 Anatolian Klasea Cass. Species," *Records of Natural Products* 10 (2016).

30. F. Bellahcene, K. Benarous, A. Mermer, et al., "Unveiling Potent Schiff Base Derivatives With Selective Xanthine Oxidase Inhibition: In Silico and In Vitro Approach," *Saudi Pharmaceutical Journal* 32 (2024): 102062, https://doi.org/10.1016/j.jsps.2024.102062.

31. R. Rullo, C. Cerchia, R. Nasso, et al., "Novel Reversible Inhibitors of Xanthine Oxidase Targeting the Active Site of the Enzyme," *Antioxidants* 12 (2023): 825, https://doi.org/10.3390/antiox12040825.

32. P. Pogodin, A. Lagunin, D. Filimonov, and V. Poroikov, "PASS Targets: Ligand-Based Multi-Target Computational System Based on a Public Data and Naïve Bayes Approach," *SAR and QSAR in Environmental Research* 26 (2015): 783–793, https://doi.org/10.1080/1062936X.2015.1078407.

33. M. L. Peach, A. V. Zakharov, R. Liu, et al., "Computational Tools and Resources for Metabolism-Related Property Predictions. 1. Overview of Publicly Available (Free and Commercial) Databases and Software," *Future Medicinal Chemistry* 4 (2012): 1907–1932, https://doi.org/10.4155/fmc.12.150.

34. M. Roman, D. L. Roman, V. Ostafe, A. Ciorsac, and A. Isvoran, "Computational Assessment of Pharmacokinetics and Biological Effects of Some Anabolic and Androgen Steroids," *Pharmaceutical Research* 35 (2018): 1–25, https://doi.org/10.1007/s11095-018-2353-1.

35. K. Murtazalieva, D. Druzhilovskiy, R. Goel, G. Sastry, and V. Poroikov, "How Good Are Publicly Available Web Services That Predict Bioactivity Profiles for Drug Repurposing?," *SAR and QSAR in Environmental Research* 28 (2017): 843–862, https://doi.org/10.1080/1062936X.2017.1399448.

36. P. G. Jamkhande, A. S. Wattamwar, S. S. Pekamwar, and P. G. Chandak, "Antioxidant, Antimicrobial Activity and In Silico PASS Prediction of *Annona reticulata* Linn. Root Extract," *Beni-Suef University Journal of Basic and Applied Sciences* 3 (2014): 140–148.

37. A. Dmitriev, D. Filimonov, A. Rudik, et al., "Drug-Drug Interaction Prediction Using PASS," *SAR and QSAR in Environmental Research* 30 (2019): 655–664, https://doi.org/10.1080/1062936X.2019.1653966.

38. A. A. Lagunin, V. I. Dubovskaja, A. V. Rudik, et al., "CLC-Pred: A Freely Available Web-Service for In Silico Prediction of Human Cell Line Cytotoxicity for Drug-Like Compounds," *PLoS ONE* 13 (2018): e0191838, https://doi.org/10.1371/journal.pone.0191838.

39. A. Rudik, A. Dmitriev, A. Lagunin, D. Filimonov, and V. Poroikov, "PASS-Based Prediction of Metabolites Detection in Biological Systems," *SAR and QSAR in Environmental Research* 30 (2019): 751–758, https://doi.org/10.1080/1062936X.2019.1665099.

40. M. De Vivo, M. Masetti, G. Bottegoni, and A. Cavalli, "Role of Molecular Dynamics and Related Methods in Drug Discovery," *Journal of Medicinal Chemistry* 59 (2016): 4035–4061, https://doi.org/10.1021/acs.jmedchem.5b01684.

41. A. Bugrim, T. Nikolskaya, and Y. Nikolsky, "Early Prediction of Drug Metabolism and Toxicity: Systems Biology Approach and Modeling," *Drug Discovery Today* 9 (2004): 127–135, https://doi.org/10.1016/S1359-6446(03)02971-4.

42. S. Schneckener, S. Grimbs, J. Hey, et al., "Prediction of Oral Bioavailability in Rats: Transferring Insights From In Vitro Correlations to (Deep) Machine Learning Models Using In Silico Model Outputs and Chemical Structure Parameters," *Journal of Chemical Information and Modeling* 59 (2019): 4893–4905, https://doi.org/10.1021/acs.jcim.9b00460.

16121880, 2026, 1, Downloaded from https://onlinelibrary.wiley.com/doi/10.1002/cbdv.202502169 by Bezm-I Alem Vakif University, Wiley Online Library on [07/01/2026]. See the Terms and Conditions (https://onlinelibrary.wiley.com/terms-and-conditions) on Wiley Online Library for rules of use; OA articles are governed by the applicable Creative Commons License

43. A. Linani, S. Bensenouci, B. I. Hafsa, et al., "In Silico Investigation of Taurodispacamide A and Strepoxazine A From *Agelas oroides* S. as Potential Inhibitors of Neuroblastoma Targets Reveals Promising Anticancer Activity," *Applied Sciences* 14 (2024): 9306, https://doi.org/10.3390/app14209306.

44. T. B. Hadda, V. Rastija, F. AlMalki, et al., "Petra/Osiris/Molinspiration and Molecular Docking Analyses of 3-Hydroxy-Indolin-2-One Derivatives as Potential Antiviral Agents," *Current Computer-Aided Drug Design* 17 (2021): 123–133, https://doi.org/10.2174/1573409916666191226110029.

45. W. Zriouel, A. Bentis, S. Majid, et al., "The Blue Tansy Essential Oil–Petra/Osiris/Molinspiration (POM) Analyses and Prediction of Its Corrosion Inhibition Performance Based on Chemical Composition," *Sustainability* 15 (2023): 14274, https://doi.org/10.3390/su151914274.

46. T. Maliar, M. Maliarová, A. Purdešová, et al., "The Adapted POM Analysis of Avenanthramides In Silico," *Pharmaceuticals* 16 (2023): 717, https://doi.org/10.3390/ph16050717.

47. A. R. Bhat, R. S. Dongre, F. A. Almalki, et al., "Synthesis, Biological Activity and POM/DFT/Docking Analyses of Annulated Pyrano[2,3-d]Pyrimidine Derivatives: Identification of Antibacterial and Antitumor Pharmacophore Sites," *Bioorganic Chemistry* 106 (2021): 104480, https://doi.org/10.1016/j.bioorg.2020.104480.

48. P. Meshram, R. Dongre, M. Ahmed, et al., "Design, Synthesis and Antibacterial Activity of New Isatin-Based Schiff Base Derivatives: Molecular Docking, POM Analysis, In Silico Pharmacokinetics and Identification of Antitumor Pharmacophore Sites," *Journal of Molecular Structure* 1322 (2025): 140508, https://doi.org/10.1016/j.molstruc.2024.140508.

49. R. Maind, S. Halder, A. R. Bhat, et al., "Phytochemical-Mediated Copper Oxide Nanoparticles Using *Cheilocostus speciosus* and *Gardenia gummifera*: Design, Synthesis, and Antimicrobial Evaluation Through In Silico and In Vitro Approaches," *ChemistrySelect* 10 (2025): e202404566, https://doi.org/10.1002/slct.202404566.

50. A. R. Bhat, S. Ahmed, and S. M. A. Kawsar, *Molecular Modeling and Docking Techniques for Drug Discovery and Design* (IGI Global, 2025).

51. X. Y. Meng, H. X. Zhang, M. Mezei, and M. Cui, "Molecular Docking: A Powerful Approach for Structure-Based Drug Discovery," *Current Computer-Aided Drug Design* 7 (2011): 146–157, https://doi.org/10.2174/157340911795677602.

52. I. A. Guedes, C. S. de Magalhães, and L. E. Dardenne, "Receptor–Ligand Molecular Docking," *Biophysical Reviews* 6 (2014): 75–87, https://doi.org/10.1007/s12551-013-0130-2.

53. X.-X. Liu, S.-W. Sun, W.-J. Yuan, et al., "Isolation of Tricin as a Xanthine Oxidase Inhibitor From Sweet White Clover (*Melilotus albus*) and Its Distribution in Selected Gramineae Species," *Molecules (Basel, Switzerland)* 23 (2018): 2719, https://doi.org/10.3390/molecules23102719.

54. K. R. Mari and S. Muthukrishnan, "Structural Characterization and In Silico Study on *Pisonia alba* Leaves Extract," *Journal of Pharmacognosy and Phytochemistry* 7 (2018): 681–693.

55. A. Linani, K. Benarous, L. Bou-Salah, M. Yousfi, and S. Goumri-Said, "Exploring Structural Mechanism of COVID-19 Treatment With Glutathione as a Potential Peptide Inhibitor to the Main Protease: Molecular Dynamics Simulation and MM/PBSA Free Energy Calculations Study," *International Journal of Peptide Research and Therapeutics* 28 (2022): 55, https://doi.org/10.1007/s10989-022-10365-6.

56. S. A. Hollingsworth and R. O. Dror, "Molecular Dynamics Simulation for All," *Neuron* 99 (2018): 1129–1143, https://doi.org/10.1016/j.neuron.2018.08.011.

57. A. Bunker and T. Róg, "Mechanistic Understanding From Molecular Dynamics Simulation in Pharmaceutical Research 1: Drug Delivery," *Frontiers in Molecular Biosciences* 7 (2020): 604770, https://doi.org/10.3389/fmolb.2020.604770.

58. M. Y. Alsedfy, A. A. Ebnalwaled, M. Moustafa, and A. H. Said, "Investigating the Binding Affinity, Molecular Dynamics, and ADMET Properties of Curcumin-IONPs as a Mucoadhesive Bioavailable Oral Treatment for Iron Deficiency Anemia," *Scientific Reports* 14 (2024): 22027, https://doi.org/10.1038/s41598-024-72577-8.

59. J. R. López-Blanco, J. I. Aliaga, E. S. Quintana-Ortí, and P. Chacón, "iMODS: Internal Coordinates Normal Mode Analysis Server," *Nucleic Acids Research* 42 (2014): W271–W276, https://doi.org/10.1093/nar/gku339.

60. M. Dhibi, Z. Amri, A. M. Bhouri, S. Hammami, and M. Hammami, "Comparative Study of the Phenolic Profile and Antioxidant Activities of Moringa (*Moringa oleifera* Lam.) and Jujube (*Ziziphus lotus* Linn.) Leaf Extracts and Their Protective Effects in Frying Stability of Corn Oil," *Measurement: Food* 7 (2022): 100045.

61. N. Malik, A. Khatkar, and P. Dhiman, "Computational Analysis and Synthesis of Syringic Acid Derivatives as Xanthine Oxidase Inhibitors," *Medicinal Chemistry Research* 16 (2020): 643–653, https://doi.org/10.2174/1573406415666191004134346.

62. M. Ishaq, L. Zhao, M. M. Soliman, et al., "Ameliorative Impacts of Sinapic Acid Against Monosodium Urate Crystal-Induced Gouty Arthritis and Inflammation Through Different Signaling Pathways," *Toxicology Research* 13 (2024): tfae130.

63. T. Dhammaraj, P. Kotseekieo, T. Chotikarn, et al., "In Vitro Investigation of Xanthine Oxidase Inhibitory and Antioxidant Activities of 3, 4, 5-Trihydroxycinnamic Acid," *Journal of Herbmed Pharmacology* 13 (2024): 439–449, https://doi.org/10.34172/jhp.2024.49420.

64. S. J. Duthie and V. L. Dobson, "Dietary Flavonoids Protect Human Colonocyte DNA From Oxidative Attack In Vitro," *European Journal of Nutrition* 38 (1999): 28–34, https://doi.org/10.1007/s003940050043.

65. L. S. Chua, "A Review on Plant-Based Rutin Extraction Methods and Its Pharmacological Activities," *Journal of Ethnopharmacology* 150 (2013): 805–817, https://doi.org/10.1016/j.jep.2013.10.036.

66. Y. Yu, Y. Xiong, S. Tong, et al., "Inhibitory Activity of Quercetin, Rutin, and Hyperoside Against Xanthine Oxidase: Kinetics, Fluorescence, and Molecular Docking," *Current Pharmaceutical Biotechnology* 26 (2025): 513–524, https://doi.org/10.2174/0113892010297269240427055003.

67. Y. Yahia, M. A. Benabderrahim, N. Tlili, M. Bagues, and K. Nagaz, "Bioactive Compounds, Antioxidant and Antimicrobial Activities of Extracts From Different Plant Parts of Two *Ziziphus* Mill. Species," *PLoS ONE* 15 (2020): e0232599, https://doi.org/10.1371/journal.pone.0232599.

68. S. Zazouli, M. Chigr, P. A. Ramos, et al., "Chemical Profile of Lipophilic Fractions of Different Parts of *Zizyphus lotus* L. by GC–MS and Evaluation of Their Antiproliferative and Antibacterial Activities," *Molecules (Basel, Switzerland)* 27 (2022): 483, https://doi.org/10.3390/molecules27020483.

69. A. Mehmood, A. U. Rehman, M. Ishaq, et al., "In Vitro and In Silico Xanthine Oxidase Inhibitory Activity of Selected Phytochemicals Widely Present in Various Edible Plants," *Combinatorial Chemistry and High Throughput Screening* 23 (2020): 917–930, https://doi.org/10.2174/1386207323666200428075224.

70. Y. Chandorkar, M. Valeske, B. Kolrosova, et al., "Bioactive Salicylic Acid Containing Coating for Dental Implants to Combat Infection and Inflammation," *Advanced Materials Interfaces* 11 (2024): 2300750, https://doi.org/10.1002/admi.202300750.

71. H. P. Song, H. Zhang, Y. Fu, et al., "Screening for Selective Inhibitors of Xanthine Oxidase From Flos Chrysanthemum Using Ultrafiltration LC–MS Combined With Enzyme Channel Blocking," *Journal of Chromatography B* 961 (2014): 56–61, https://doi.org/10.1016/j.jchromb.2014.05.001.

72. M. E. M. B. de Araújo, Y. E. M. Franco, T. G. Alberto, et al., "Kinetic Study on the Inhibition of Xanthine Oxidase by Acylated Derivatives of Flavonoids Synthesised Enzymatically," *Journal of Enzyme Inhibition and Medicinal Chemistry* 32 (2017): 978–985, https://doi.org/10.1080/14756366.2017.1347165.

73. S. Adachi, M. Oyama, S. Kondo, and K. Yagasaki, "Comparative Effects of Quercetin, Luteolin, Apigenin and Their Related Polyphenols on Uric Acid Production in Cultured Hepatocytes and Suppression of Purine

16121880, 2026, 1, Downloaded from https://onlinelibrary.wiley.com/doi/10.1002/cbdv.202502169 by Beam-I Aben Vakf University, Wiley Online Library on [07/01/2026]. See the Terms and Conditions (https://onlinelibrary.wiley.com/terms-and-conditions) on Wiley Online Library for rules of use; OA articles are governed by the applicable Creative Commons License

Bodies-Induced Hyperuricemia by Rutin in Mice," *Cytotechnology* 73 (2021): 343–351, https://doi.org/10.1007/s10616-021-00452-9.

74. J. M. Pauff and R. Hille, "Inhibition Studies of Bovine Xanthine Oxidase by Luteolin, Silibinin, Quercetin, and Curcumin," *Journal of Natural Products* 72 (2009): 725–731, https://doi.org/10.1021/np8007123.

75. O. Balázs, Á. Dombi, B. Z. Zsidó, et al., "Inhibition of Xanthine Oxidase-Catalyzed Xanthine and 6-Mercaptopurine Oxidation by Luteolin, Naringenin, Myricetin, Ampelopsin and Their Conjugated Metabolites," *Biomedicine & Pharmacotherapy* 167 (2023): 115548, https://doi.org/10.1016/j.biopha.2023.115548.

76. Z. Calis, D. Dasdelen, A. K. Baltaci, and R. Mogulkoc, "Naringenin Prevents Renal Injury in Experimental Hyperuricemia Through Suppressing Xanthine Oxidase, Inflammation, Apoptotic Pathway, DNA Damage, and Activating Antioxidant System," *Metabolic Syndrome and Related Disorders* 21 (2023): 275–281, https://doi.org/10.1089/met.2023.0012.

77. N. Bencheikh, M. Bouhrim, L. Kharchoufa, et al., "The Nephroprotective Effect of *Zizyphus lotus* L.(Desf.) Fruits in a Gentamicin-Induced Acute Kidney Injury Model in Rats: A Biochemical and Histopathological Investigation," *Molecules (Basel, Switzerland)* 26 (2021): 4806, https://doi.org/10.3390/molecules26164806.

78. L. Duan, W. Ding, X. Liu, et al., "Biosynthesis and Engineering of Kaempferol in Saccharomyces Cerevisiae," *Microbial Cell Factories* 16 (2017): 165, https://doi.org/10.1186/s12934-017-0774-x.

79. M. L. Falcone Ferreyra, S. P. Rius, and P. Casati, "Flavonoids: Biosynthesis, Biological Functions, and Biotechnological Applications," *Frontiers in Plant Science* 3 (2012): 222, https://doi.org/10.3389/fpls.2012.00222.

80. S. A. Rodriguez, A. P. Murray, and J. M. Leiro, "Xanthine Oxidase Inhibition by Aqueous Extract of *Limonium brasiliense* (Plumbaginaceae)," *Chemistry Proceedings* 3 (2021): 123.

81. R. A. El-Shiekh, M. H. Radi, and E. Abdel-Sattar, "Unveiling the Therapeutic Potential of Aromadendrin (AMD): A Promising Anti-Inflammatory Agent in the Prevention of Chronic Diseases," *Inflammopharmacology* 33 (2025): 1209–1220, https://doi.org/10.1007/s10787-025-01647-8.

82. Y. Wan, F. Wang, B. Zou, et al., "Molecular Mechanism Underlying the Ability of Caffeic Acid to Decrease Uric Acid Levels in Hyperuricemia Rats," *Journal of Functional Foods* 57 (2019): 150–156, https://doi.org/10.1016/j.jff.2019.03.038.

83. C. Alla, A. Ali, A. Mehiou, et al., "Phytochemical Composition of *Ziziphus lotus* (L.) Lam and Its Impact on the Metabolic Syndrome: A Review," *Advances in Pharmacological and Pharmaceutical Sciences* 2025 (2025): 8276090, https://doi.org/10.1155/adpp/8276090.

84. J. Sharifi-Rad, F. Kobarfard, A. Ata, et al., "Prosopis Plant Chemical Composition and Pharmacological Attributes: Targeting Clinical Studies From Preclinical Evidence," *Biomolecules* 9 (2019): 177.

85. R. Ben Ammar, S. Kilani, I. Bouhlel, et al., "Antiproliferative, Antioxidant, and Antimutagenic Activities of Flavonoid-Enriched Extracts From (Tunisian) *Rhamnus alaternus* L.: Combination With the Phytochemical Composition," *Drug and Chemical Toxicology* 31 (2008): 61–80, https://doi.org/10.1080/01480540701688725.

86. E. R. Elsharkawy, F. Almalki, T. Ben Hadda, V. Rastija, H. Lafridi, and H. Zgou, "DFT Calculations and POM Analyses of Cytotoxicity of Some Flavonoids From Aerial Parts of *Cupressus sempervirens*: Docking and Identification of Pharmacophore Sites," *Bioorganic Chemistry* 100 (2020): 103850, https://doi.org/10.1016/j.bioorg.2020.103850.

87. S. Nadeem, M. Sirajuddin, S. Ahmad, S. A. Tirmizi, M. I. Ali, and A. Hameed, "Synthesis, Spectral Characterization and In Vitro Antibacterial Evaluation and Petra/Osiris/Molinspiration Analyses of New Palladium (II) Iodide Complexes With Thioamides," *Alexandria Journal of Medicine* 52 (2016): 279–288, https://doi.org/10.1016/j.ajme.2015.10.003.

88. P. Subash-Babu, S. Abdulaziz AlSedairy, M. Abdulaziz Binobead, and A. A. Alshatwi, "Luteolin-7-*O*-Rutinoside Protects RIN-5F Cells From High-Glucose-Induced Toxicity, Improves Glucose Homeostasis in L6 Myotubes, and Prevents Onset of Type 2 Diabetes," *Metabolites* 13 (2023): 269.

16121880, 2026, 1, Downloaded from https://onlinelibrary.wiley.com/doi/10.1002/cbdv.202502169 by Bezm-I Alem Vakif University, Wiley Online Library on [07/01/2026]. See the Terms and Conditions (https://onlinelibrary.wiley.com/terms-and-conditions) on Wiley Online Library for rules of use; OA articles are governed by the applicable Creative Commons License